The Egyptian Journal of Radiology and Nuclear Medicine (2015) **46**, 339–354

Egyptian Society of Radiology and Nuclear Medicine

The Egyptian Journal of Radiology and Nuclear Medicine

www.elsevier.com/locate/ejrnm
www.sciencedirect.com

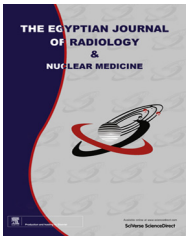

REVIEW

Alternative technique using dual source CT imaging for assessment of myocardial perfusion

Amgad S. Abdel-Rahman *, **Heba I. Aly, Mohamed A. Saleh, Ahmed S. Ibrahim, Hanan M.H. Arafa**

Radiology Department, Faculty of Medicine, Ain Shams University, Cairo, Egypt

Received 15 October 2014; accepted 13 January 2015
Available online 10 February 2015

KEYWORDS

Dual source computed tomography (DSCT);
Computed tomography perfusion (CTP);
Coronary CT angiography (cCTA);
Coronary artery disease (CAD);
Myocardial infarction (MI)

Abstract *Purpose:* To elucidate the diagnostic role of multidetector DSCT for the assessment of myocardial perfusion in correlation with coronary luminal integrity in a single CT scan while both tubes were operated in single energy mode.
Methods and material: Thirty-five patients were subjected to single acquisition contrast-enhanced, ECG-gated DSCT of the heart at rest. Postprocessing was performed generating two image sets: coronary CT angiographic images (cCTA) and myocardial perfusion images (CTP) for respective correlative assessment of coronary luminal integrity and myocardial perfusion. Perfusion defect was detected subjectively using gray scale images and the color coded first pass and color overlaid late enhancement (color attenuation) images were used for semi-objective evaluation and final objective and quantitative confirmation by density measurement.
Results: Significant correlation and good agreement between the findings of DSCT myocardial perfusion and the findings of stenosis and its degree on cCTA on a segmental basis is noted with Cohen's Kappa = 0.67 and prevalence and bias adjusted Kappa = 0.71 emphasizing the high diagnostic value of DSCT myocardial perfusion as compared to cCTA as the gold reference standard.
Conclusion: We propose that comprehensive evaluation of coronary artery morphology and myocardial perfusion in patients with CAD could be achieved by single reproducible non-invasive contrast enhanced CT acquisition using DSCT scanners while operated in single energy mode with high sensitivity, specificity and diagnostic accuracy, it also has the potential to be the first, independent and stand out imaging choice in such field.
© 2015 The Egyptian Society of Radiology and Nuclear Medicine. Production and hosting by Elsevier B.V. This is an open access article under the CC BY-NC-ND license (http://creativecommons.org/licenses/by-nc-nd/4.0/).

* Corresponding author.
Peer review under responsibility of Egyptian Society of Radiology and Nuclear Medicine.

http://dx.doi.org/10.1016/j.ejrnm.2015.01.003
0378-603X © 2015 The Egyptian Society of Radiology and Nuclear Medicine. Production and hosting by Elsevier B.V.
This is an open access article under the CC BY-NC-ND license (http://creativecommons.org/licenses/by-nc-nd/4.0/).

Contents

1. Introduction

400,000 patients per year experience ST segment elevation myocardial infarction (MI) in the United States (1). Patients who pass acute MI without death face a high risk of many cardiac complications including angina pectoris, heart failure, stroke, recurrent acute MI and sudden death (2). Patients with coronary artery disease (CAD) may present with many symptoms and complications such as unstable angina, non-fatal myocardial infarction and sudden death (3) and it leads to chronic heart failure and decreased ejection fraction (EF) (4) because, with time, global ventricular dysfunction may complicate regional myocardial dysfunction (5). Comprehensive assessment of coronary arterial luminal integrity, size of infarction as well as regional and global function of the left ventricle is mandatory for risk stratification, prognosis and hence, better management. Many examinations including echo-cardiography and myocardial perfusion imaging such as SPECT; single photon emission computed tomography and MRI; magnetic resonance imaging, as well as the conventional invasive coronary angiography could be employed to collect this information which may consume time and efforts (6). Multi-detector computed tomography technology showed progressive improvements with sub-millimeter collimation and fast gantry rotation which enabled comprehensive cardiac evaluation with assessment of regional and global left ventricular function as well as left ventricular perfusion status beside the non-invasive assessment of the coronary luminal integrity. Many studies showed high diagnostic sensitivity, specificity and accuracy of the multi-detector CT in detection of significant coronary arteries lesions when compared to conventional invasive coronary angiography (7) while reports regarding multi-detector CT assessment of left ventricular wall motion abnormalities and function as well as detection of perfusion defects in acute myocardial infarction are limited. Multi-detector CT comprehensive assessment of the heart and coronary arteries should rise as a non-invasive study for patients with acute myocardial infarction if it could evaluate these issues (6). We aimed in this study to elucidate role of multi-detector DSCT for the assessment of myocardial perfusion being essential for prognosis and for evaluating therapeutic responses.

2. Material and methods

2.1. Study population

The study population involved 35 patients who had performed DSCT coronary angiography study in some private hospital in east of Cairo, Egypt. All patients were complaining of cardiovascular symptoms including chest pain and were requested to do the study by their physicians who were either suspecting CAD or following up a known CAD. Approval of the Ethical committee of scientific Research, faculty of medicine, Ain Shams University was gained before the study commences.

Both sexes were included in the study with no age predilection. Patients with previous coronary artery bypass grafting or per-cutaneous coronary intervention were excluded as well as patients with bad general condition needing life support and those with severe hepato-renal disease. Also, pregnant females and patients known to have high serum creatinine level are excluded as well as patients with history of allergy to iodinated contrast material or history of reactive airway disease.

2.2. Patient's preparation

Clinical evaluation was done and the patients were instructed to fast for at least six hours. Administration of one ante-cubital 18–20-gauge intravenous catheter and detailed explanation

of imaging procedure, including practicing of breath holds were done. In cases where heart rate was more than 70 beats per minute and there was no contraindication to use β-blockers, 50 gm tablet of atenolol Ph. Eur., β1-selective (cardioselective) blocker, (Tenormin, AstraZeneca) was given orally to the patient 30 min. before the study. Finally electro-cardiographic electrodes were placed on the patient's chest.

2.3. DSCT protocol

Fast dual-source CT system (Somatom Definition Flash; Siemens Healthcare, Forchheim, Germany) was used. This machine employs 2 X-ray tubes and detector banks (128 detector rows) mounted in a perpendicular fashion to each other in the same gantry with 256 effective detector rows. Due to unavailability of Heart PBV cardiac CT perfusion analysis software, we operated the CT scanner only in single energy mode and we used the available basic perfusion software. Single CT acquisition was obtained at rest with the following parameters: 280 ms gantry rotation time, pitch of 0.18, $128 \times 2 \times 0.6$ mm collimation with *z*-flying focal spot technique and 75 ms temporal resolution. Both tubes were operated with 150–400 mAs/rot at 120 kV.

2.4. Image acquisition

The patient was positioned supine on CT table and was attached to cardiac rhythm monitor. Scout image was acquired to localize the heart position. Dynamic first-pass myocardial CT perfusion imaging was performed during rest. Data were acquired in a cranio-caudal direction with simultaneous recording of the patient's ECG signal in order to allow for retrospective registration of image reconstruction to the desired cardiac phase. The anatomical range extended from the level of the carina to just below the dome of the diaphragm. Throughout the study, ECG readings, patient's heart rate and rhythm were monitored. The radiation exposure was calculated based on the individual CT parameters in each patient.

2.5. Contrast material

Contrast enhancement was achieved with nonionic iodinated contrast medium (Scanlux, 370 mgI/ml iopamidol, Sanochemia Pharmazeutika AG, Boltzmanngasse) which was injected through the antecubital vein catheter with a flow of 6 mL/s. A biphasic injection protocol was used: a bolus of 75 mL of pure contrast medium in the first phase followed by 40 mL of normal saline chaser bolus in the second phase using a dual-syringe injector (Stellant D; Medrad, Indianola, PA). Scan delay time was determined with the test bolus technique using 15 mL of contrast material bolus followed by a bolus of 30 mL of normal saline, both injected at a rate of 6 mL/s. The timing was calculated by adding 2 s to the time of peak contrast enhancement in the ascending aorta (measured at the level of the aortic root by repetitive scanning) in order to achieve sufficient perfusion of contrast material throughout the myocardium.

2.6. DSCT data postprocessing and image interpretation

2.6.1. Postprocessing

Postprocessing using various postprocessing algorithms and image analysis were performed on an online remote workstation (Syngo.via version VA11A; Siemens Healthcare, Forchheim, Germany) by using a commercially available dedicated software tool. The most useful algorithms were multiplanar reformatting (MPR), curved multi-planar reformatting (cMPR), maximum intensity projection (MIP) and volume rendering (VR).

Clinical cCTA analysis of coronary artery morphology for stenosis detection and grading was performed using the automatically or semi-automatically generated curved multiplanar reformats of the target vessels. Grading of stenosis severity in a quantitative manner was done using the semi-automated vessel analysis tool that reconstructs cross-sectional images perpendicular to the long axis of the target artery and so determines luminal diameters and cross-sectional area that enable stenosis percentage calculation. Angiographic images were reconstructed in the best diastolic phase using retrospective ECG gating. Image reconstruction was performed with 0.75 mm reconstructed section width and 0.4 mm reconstruction increment using the routine reconstruction algorithm implemented on the scanner platform. Evaluation of cCTA was done in consensus having the agreement that stenosis $> 50\%$ was to be considered as hemodynamically significant.

Perfusion images were reconstructed with a 0.7 mm section width every 0.4 mm in multiplanar reformats, with short-axis, vertical long axis and horizontal long axis sections reconstructed during middiastole to minimize motion artifacts. Evaluation of myocardial perfusion images was based on relative difference in iodinated contrast material contained blood that is perfused into the myocardium which explains the direct relationship between the amount of perfused contrast material within the myocardium and myocardial enhancement and, subsequently, its attenuation in Hounsfield unit (HU).

So, hypo-perfused area of myocardium named perfusion defect (PD) had a remarkably lower attenuation which could be detected visually (subjectively) in gray scale images, semi-objectively with the help of the color coded first pass and color overlaid late enhancement (color attenuation) images and, finally, was confirmed quantitatively (objectively) by measuring attenuation in HU by placing region of interest (ROI). The observers evaluated the gray scale images for subjective detection of areas of hypo-perfusion, with manipulation (narrowing) of window level and width (width around 200 HU and level around 100 HU). Then, they evaluated the color attenuation images that highlight the hypo-perfused areas by a recognizable color in a semi-objective way using the dedicated post-processing software tools. Finally, they confirmed the hypo-perfused areas by drawing regions of interest of comparative areas in the hypo-perfused areas and other normally perfused reference areas to compare between their numerical density values in Hounsfield unit (HU). This way emphasizes the diagnosis of the hypo-perfused areas in a quantitative objective way.

Coronary CT angiography (cCTA) was used as the final reference standard for validating myocardial blood-pool deficits on DSCT. Coronary vessel dominance was observed to determine which coronary artery is supplying the inferior and inferoseptal territories and to ensure the accurate matching of myocardial segments with the associated vascular territory. Left ventricular (LV) systolic contractility and regional wall motion (RWM) assessment were performed by evaluating the reconstructed short axis images in end diastolic and end systolic phases as well as in cine mode and 17 segments chart.

Table 1 Results of cCTA.

Variable	Number	Percent
Coronary vessel with significant lesion by cCTA		
RCA	9	25.7
LAD	27	77.1
LCx	15	42.9
Number of vessels with significant lesion by cCTA		
Nil	5	14.3
One	14	40.0
Two	11	31.4
Three	5	14.3

Global LV function (ejection fraction (EF), end-diastolic volume and end-systolic volume) was automatically calculated by the appropriate software tool built in the workstation. The results were collected and statistically analyzed.

2.7. Statistical methods

Statistical analysis was done using IBM© SPSS© Statistics version 20 (IBM© Corp., Armonk, NY, USA), MedCalc© version 12.5 (MedCalc© Software bvba, Ostend, Belgium), and DAG Stat spreadsheet (8).

Normally distributed quantitative variables were presented as mean and SD. Skewed variables were presented as percentiles. The diagnostic value of DSCT myocardial perfusion was contrasted against that of cCT angiography as a gold-standard test. The following diagnostic indices were calculated: sensitivity, specificity, Youden's index, accuracy (correct classification rate), positive predictive value and negative predictive value.

Agreement between various tools for binary outcomes was assessed using Cohen's kappa (κ) and the prevalence-adjusted and bias-adjusted kappa (PABAK). For ordinal outcomes, the intra-class correlation coefficient (ICC) was calculated. Inter-group comparisons for quantitative variables were done using the Mann–Whitney *U*-test with application of the Bonferroni method to correct for multiple comparisons. *P*-values < 0.05 were considered statistically significant. For multiple comparison, this was equivalent to a Bonferroni-adjusted value of $p < 0.017$.

3. Results

The studied population included 35 patients, 8 females (22.9%) and 27 males (77.1%). The mean age was 60 ± 7.4 years ranging from 42 to 73 years. 54.3% (19/35) of the studied population are hypertensive, 31.4% (11/35) had diabetes mellitus, 22.9% (8/35) had dyslipidemia and 20% (7/35) were former or current smokers.

3.1. Coronary CTA (cCTA) Data

Coronary CTA (cCTA) revealed significant (>50% luminal area reduction) coronary artery stenosis in 30 patients out of thirty-five patients. 9/30 (25.7%) patients had significant stenosis in the right coronary artery territory, 27/30 (77.1%) patients had significant stenosis in the left anterior descending (LAD) territory and 15/30 (42.9%) patients had significant stenosis in the left circumflex (LCx) territory. Fourteen patients (40%) had single coronary artery significant stenosis, 11 patients (31.4%) had two coronary arteries significant stenosis and 5 patients (14.3%) had three coronary arteries significant stenosis (Table 1).

Table 2 Density values in hypo-perfused and reference normally perfused areas.

Variable	n.	Min.	Max.	Mean	SD	Percentiles		
						25th	50th	75th
Density in hypo-perfused areas in RCA territory (HU)	9	19.0	75.0	39.7	19.1	25.5	33.0	55.0
Density in hypo-perfused areas in LAD territory (HU)	27	18.0	73.0	43.2	12.7	37.0	42.0	52.0
Density in hypo-perfused areas in LCx territory (HU)	15	23.0	59.0	40.9	9.2	36.0	38.0	48.0
Density in reference area 1 (HU)	35	70.0	211.0	98.9	24.3	87.0	94.0	109.0
Density in reference area 2 (HU)	35	68.0	135.0	97.5	15.6	85.0	99.0	108.0
Density in reference area 3 (HU)	35	66.0	212.0	99.4	24.1	87.0	95.0	107.0
Average density in reference areas (HU)	35	68.3	186.0	98.6	20.4	85.7	97.0	107.7

Table 3 Comparison between density in hypo-perfused territories and reference density in normally perfused myocardium.

	Reference density	Density in RCA territory hypo-perfused area	Density in LAD territory hypo-perfused area	Density in LCx territory hypo-perfused area
Sample size	35	9	27	15
Lowest value	68.3	19	18	23
Highest value	186	75	73	59
Median	97	33	42	38
Interquartile range	86.0–107.4	25.8–50.0	37.5–50.5	36.0–46.8
p-Value versus reference	–	<0.0001	<0.0001	<0.0001

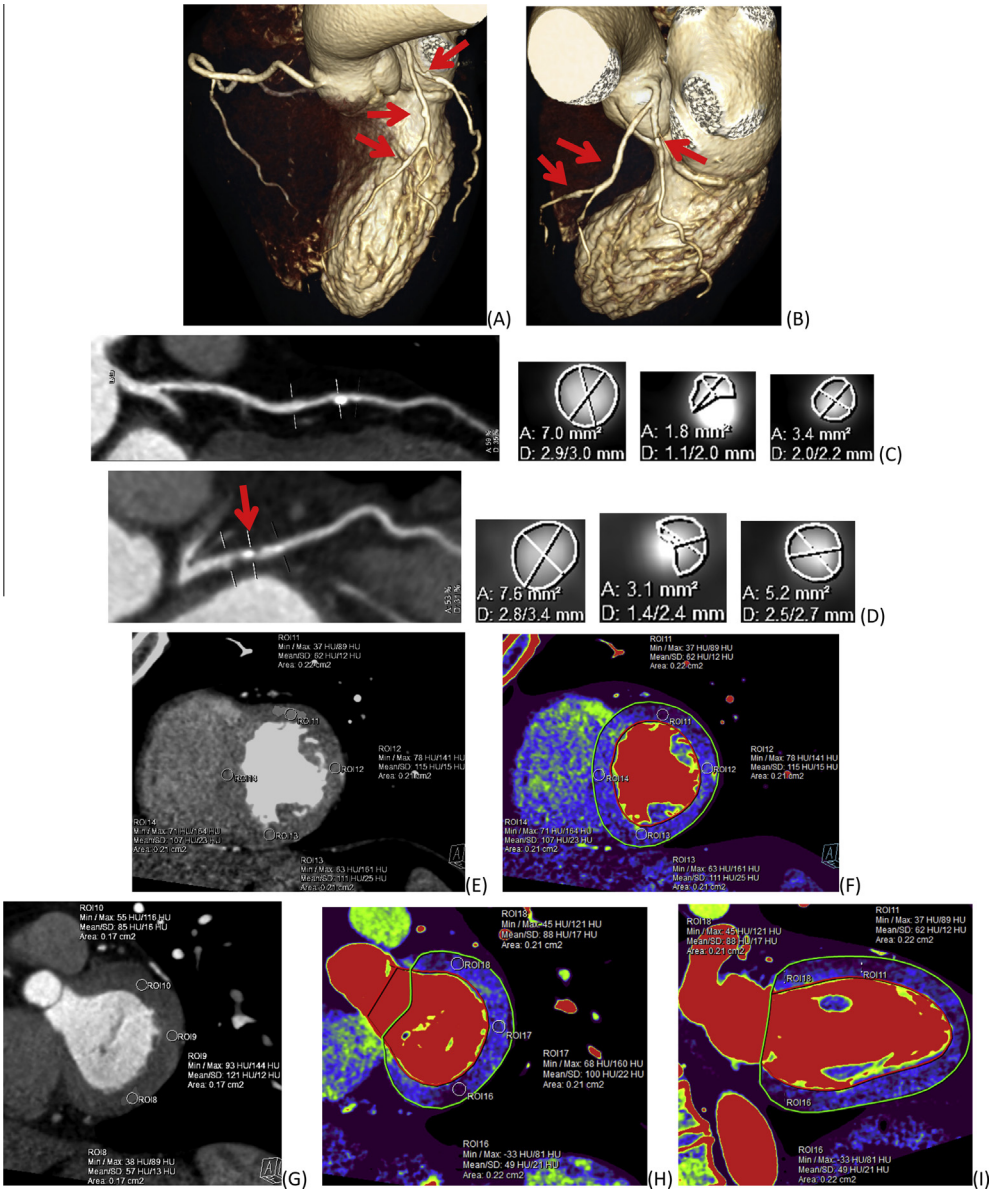

Fig. 1 A 52 year old hypertensive male patient with known CAD presented by chest pain. Blood pool volume rendered images of cardiac right anterior aspect in (A) and cardiac left anterior aspect in (B) showing surface irregularities of the coronary arteries with contour bulges at the proximal part of LCx and middle part of LAD (red arrows). (C) cMPR image of LAD showing calcified plaque at its middle segment which is also used to locate reference lines before, at and after the plaque for cross-sectional assessment images creation revealing luminal area of 7, 1.8 and 3.4 mm^2, respectively, accounting for 59% luminal area narrowing at the plaque site. (D) cMPR image of LCx showing predominantly calcified plaque at its proximal part which is also used to locate reference lines before, at and after the plaque for cross-sectional assessment images creation revealing luminal area of 7.6, 3.1 and 5.2 mm^2, respectively, accounting for 53% luminal area narrowing at the plaque site. (E) Short axis image with applied first pass enhancement tool showing anterior wall myocardial hypo-perfused area that is highlighted by light gray shade. (F) Short axis image at the same level as (E) with applied late enhancement tool demonstrating the anterior wall myocardial hypo-perfused area that takes deep blue color as compared to the surrounding normally perfused myocardium taking light blue or green color. In E and F images added ROIs at anterior wall hypo-perfused area, lateral, posterior and septal walls of the left ventricle show low mean density at the hypo-perfused area, 62 HU as compared to mean density of other ROIs measuring 115, 111, 107 HU, respectively. (G) Short axis image at left ventricular basal segment with applied first pass enhancement toll showing postero-lateral wall myocardial hypo-perfused area that is highlighted by light gray shade. (H) Short axis image at the same level as (G) with applied late enhancement tool demonstrating the postero-lateral wall myocardial hypo-perfused area in deep blue color. In G and H images added ROIs at postero-lateral wall hypo-perfused area, lateral and anterior walls of the left ventricle show low mean density at the hypo-perfused area, 49 HU as compared to mean density of other ROIs measuring 100 and 88 HU, respectively. (I) Vertical long axis image with applied late enhancement tool showing the previously demonstrated anterior wall midsegment and postero-lateral wall basal segment myocardial hypo-perfused areas in deep blue color.

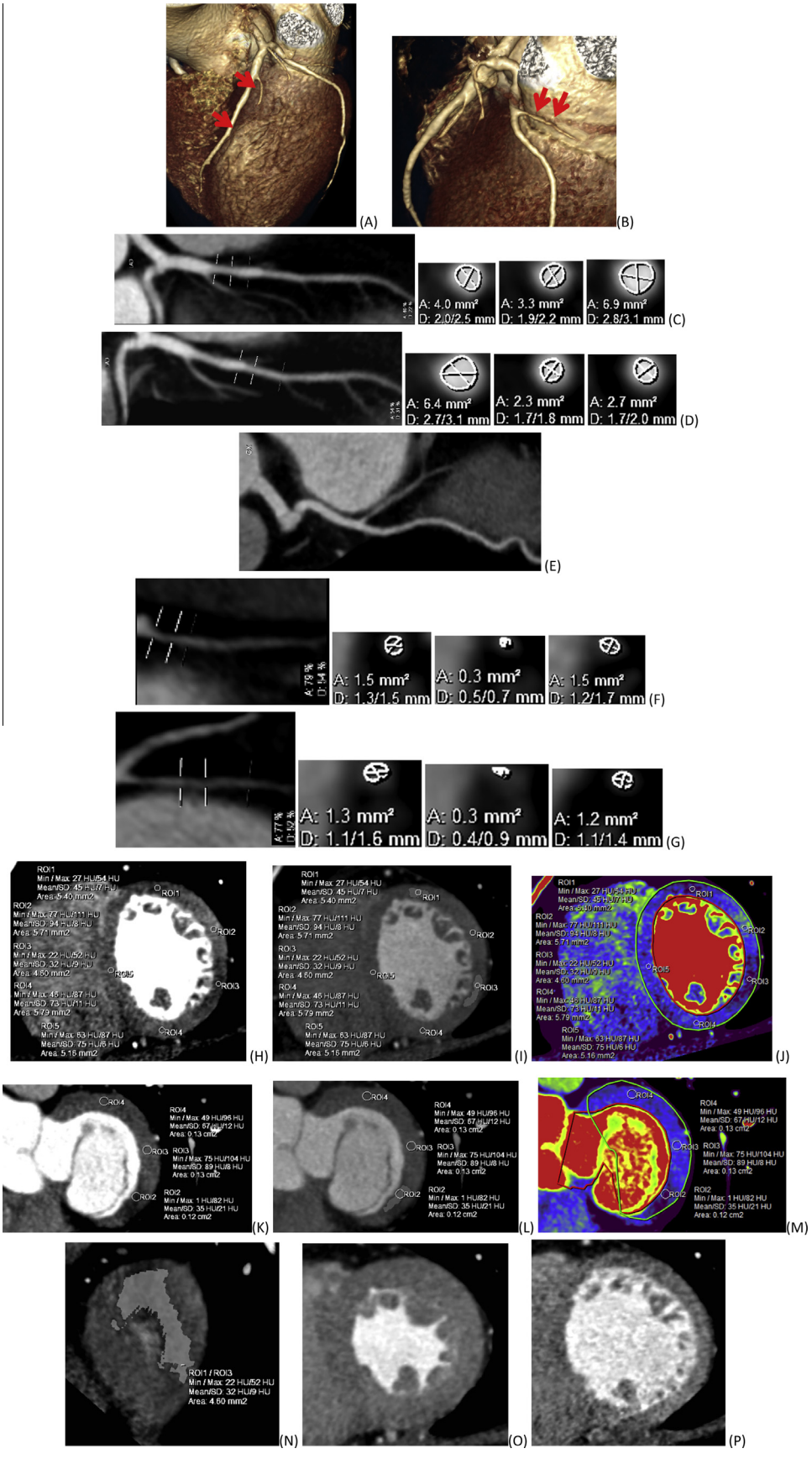
(A)
(B)
A: 4.0 mm²
D: 2.0/2.5 mm
A: 3.3 mm²
D: 1.9/2.2 mm
A: 6.9 mm²
D: 2.8/3.1 mm
(C)
A: 6.4 mm²
D: 2.7/3.1 mm
A: 2.3 mm²
D: 1.7/1.8 mm
A: 2.7 mm²
D: 1.7/2.0 mm
(D)
(E)
A: 1.5 mm²
D: 1.3/1.5 mm
A: 0.3 mm²
D: 0.5/0.7 mm
A: 1.5 mm²
D: 1.2/1.7 mm
(F)
A: 1.3 mm²
D: 1.1/1.6 mm
A: 0.3 mm²
D: 0.4/0.9 mm
A: 1.2 mm²
D: 1.1/1.4 mm
(G)
(H)
(I)
(J)
(K)
(L)
(M)
ROI1 / ROI3
Min / Max: 22 HU/52 HU
Mean/SD: 32 HU/9 HU
Area: 4.60 mm2
(N)
(O)
(P)

3.2. Dual-source CT myocardial perfusion data

From the study population (35 patients), 595 myocardial segments were evaluated, from which 209 segments in 30 patients showed myocardial perfusion defect on DSCT and the remaining 386 segments showed no myocardial perfusion defects.

Summary of the measured myocardial density values in hypo-perfused and other normally perfused reference areas as well as comparison between them is shown in Tables 2 and 3.

3.3. Correlative analysis of dual-source CT myocardial perfusion and cCTA data

Correlation of myocardial perfusion images for perfusion defects with the cCTA images for supplying coronary artery significant stenosis in a territorial base was done and demonstrated myocardial perfusion defect in the inferior myocardial wall and inferior septum in cases with significant right coronary artery affection, myocardial perfusion defect in the anterior wall and anterior septum in cases with significant LAD artery affection and myocardial perfusion defect in the lateral wall in cases with significant LCx artery affection, except for one case that showed perfusion defect in lateral as well as inferior walls in a patient with LCx artery dominance.

355/386 segments that showed no myocardial perfusion defect were supplied by a coronary artery showing no or insignificant ($< 50\%$) stenosis and 31/386 segments that showed no myocardial perfusion defects were supplied by a coronary artery with $> 50\%$ (significant) stenosis (see Figs. 1–5).

Table 4 and Fig. 6 summarize the correlative data of both cCTA and related territorial myocardial perfusion and show their statistical analysis elucidating the diagnostic value of DSCT myocardial perfusion as compared to cCTA as the gold reference standard.

The correlative data analysis revealed high diagnostic value of DSCT myocardial perfusion in detection of myocardial segments with perfusion defects as compared to cCTA on a segmental basis as the gold standard reference with overall 83% sensitivity, 87% specificity, 86% accuracy, 70% Youden's index with 74% positive predictive value and 92% negative predictive value.

It also showed a good agreement between findings of DSCT myocardial perfusion and cCTA (0.67 Cohen's Kappa and 0.71 Prevalence and bias adjusted Kappa).

3.4. Dual-source CT kinetic and left ventricular function assessment

From the thirty patients that showed perfusion defect consequent to supplying coronary artery significant stenosis, 16

Fig. 2 A 59 year old Diabetic male patient with known CAD is presented with chest pain with exercise. Volume rendered images of cardiac anterior aspect in (A), left antero-lateral aspect in (B) showing mild atherosclerotic changes with mild surface irregularities and contour bulges. Image (A) shows trifurcation of the LMCA into LAD, LCx and short atherosclerotic ramus intermedius branch, also it shows LAD middle segment caliber irregularities (red arrows). Image (B) shows LCx artery giving a large OM branch and continues as a short vessel that shows luminal caliber irregularities (red arrows). (C) cMPR image of LAD showing 2 stenoses at its middle segment which is also used to locate reference lines before, at and after the first stenosis for cross-sectional assessment images creation revealing luminal area of 4, 3.3 and 6.9 mm^2, respectively, accounting for 40% luminal area narrowing. (D) cMPR image of LAD which is also used to locate reference lines before, at and after the second stenosis for cross-sectional assessment images creation revealing luminal area of 6.7, 2.3 and 2.7 mm^2, respectively, which account for 54% luminal area narrowing. (E) cMPR image of LCx that gives a large OM branch and continues as a short small vessel which shows caliber irregularities. (F) cMPR image of LCx short small continuation which is also used to locate reference lines before, at and after the stenosis seen just after giving the large OM branch for cross-sectional assessment images creation revealing luminal area of 1.5, 0.3 and 1.5 mm^2, respectively, accounting for 79% luminal area narrowing. (G) cMPR image of LCx which is used to locate reference lines before, at and after the second stenosis for cross-sectional assessment images creation revealing luminal area of 1.3, 0.3 and 1.2 mm^2, respectively, accounting for 77% luminal area narrowing. (H) Short axis gray scale image at midleft ventricle after narrowing WW and WL (WW: 246 and WL: 94) showing anterior and lateral walls hypo-dense areas of hypo-perfusion. (I) Short axis image with applied first pass enhancement tool at the same level as H image emphasizing the anterior and lateral walls myocardial hypo-perfused areas that are highlighted by light gray shade. (J) Short axis image with applied late enhancement tool at the same level as H and I images demonstrating the anterior and lateral walls myocardial hypo-perfused areas as areas of deep blue color as compared to the surrounding normally perfused myocardium taking light blue or green color. In H, I and J images added ROIs at the anterior and lateral walls hypo-perfused areas as well as at normally perfused areas on lateral, posterior and septal walls of the left ventricle showing low mean density at the hypo-perfused areas, 45 and 32 HU, respectively as compared to mean density of other ROIs measuring 94, 73 and 75 HU, respectively. (K) Short axis gray scale image at left ventricle base after narrowing WW and WL (WW: 299 and WL: 129) showing lateral wall posterior part hypo-dense area of hypo-perfusion. (L) Short axis image with applied first pass enhancement tool at the same level as K image emphasizing the lateral wall myocardial hypo-perfused area that is highlighted by light gray shade. (M) Short axis image with applied late enhancement tool at the same level as K and L images demonstrating the lateral wall myocardial hypo-perfused area as area of deep blue color. In K, L and M images added ROIs at the lateral wall hypo-perfused area as well as at normally perfused areas on anterior and lateral walls of the left ventricle showing low mean density at the hypo-perfused area, 35 HU, respectively as compared to mean density of other ROIs measuring 67 and 89 HU, respectively. (N) Oblique vertical long axis image at the most lateral portion of the left ventricle (lateral wall posterior part) with applied first pass enhancement tool showing the extent of lateral wall myocardial hypo-perfused area which is highlighted by light gray shade. (O and P) Short axis gray scale images at left ventricular midsegment level at end-systole and end-diastole, respectively, showing normal kinesia of left ventricle walls.

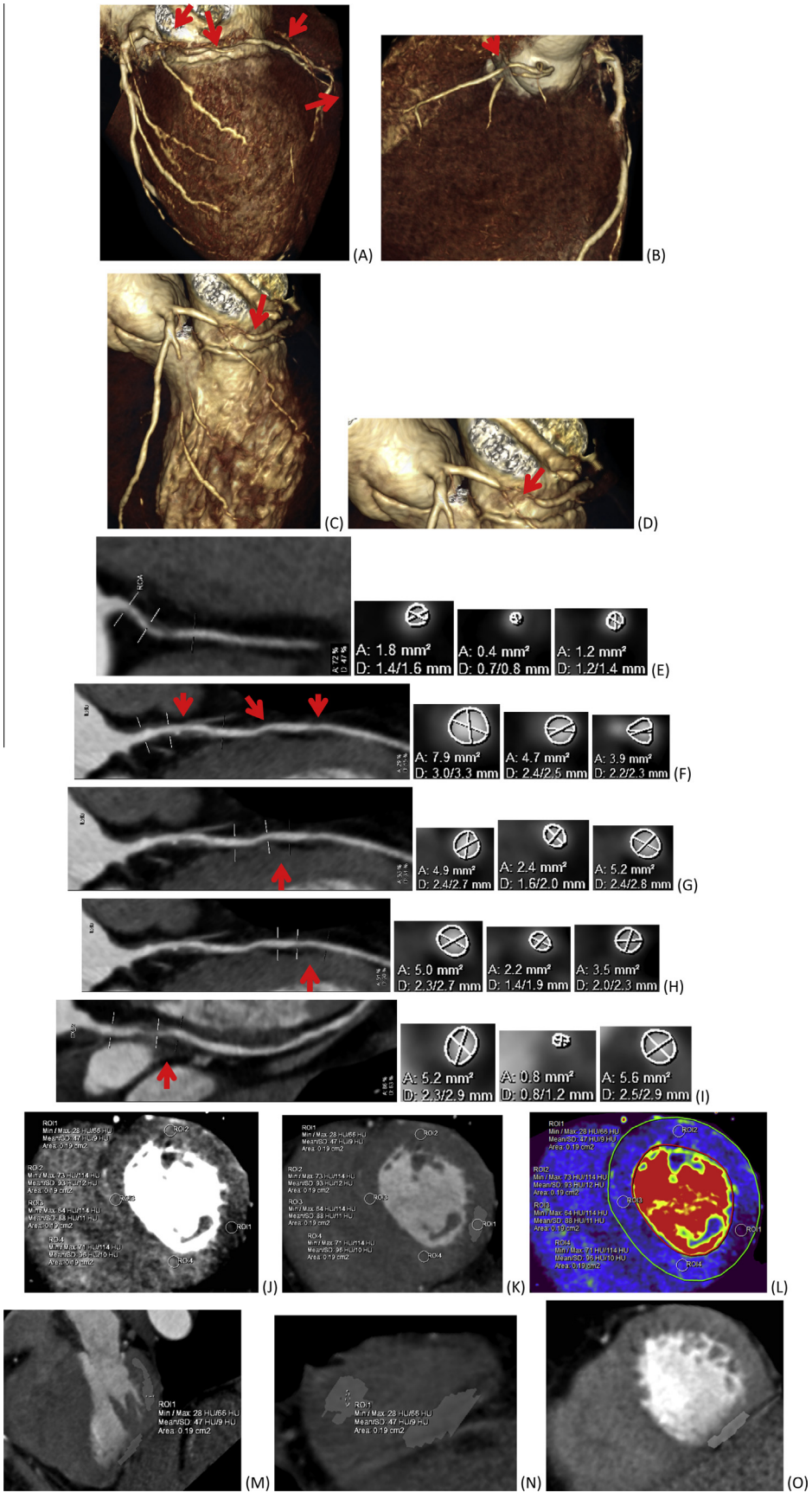
(A)
(B)
(C)
(D)
A: 1.8 mm²
D: 1.4/1.6 mm
A: 0.4 mm²
D: 0.7/0.8 mm
A: 1.2 mm²
D: 1.2/1.4 mm
(E)
A: 7.9 mm²
D: 3.0/3.3 mm
A: 4.7 mm²
D: 2.4/2.5 mm
A: 3.9 mm²
D: 2.2/2.3 mm
(F)
A: 4.9 mm²
D: 2.4/2.7 mm
A: 2.4 mm²
D: 1.6/2.0 mm
A: 5.2 mm²
D: 2.4/2.8 mm
(G)
A: 5.0 mm²
D: 2.3/2.7 mm
A: 2.2 mm²
D: 1.4/1.9 mm
A: 3.5 mm²
D: 2.0/2.3 mm
(H)
A: 5.2 mm²
D: 2.3/2.9 mm
A: 0.8 mm²
D: 0.8/1.2 mm
A: 5.6 mm²
D: 2.5/2.9 mm
(I)
(J)
(K)
(L)
(M)
(N)
(O)

patients showed kinetic abnormalities. 4/16 patients had kinetic abnormalities in the right coronary artery territory, 14/16 patients had kinetic abnormalities in the LAD artery territory and 6/16 patients had kinetic abnormalities in the LCx artery territory. 10 patients had kinetic abnormality in single territory, 4 patients had kinetic abnormality in two territories and 2 patients had kinetic abnormality in the three territories.

From the 30 patients who showed significant coronary artery stenosis and related territorial myocardial perfusion defects, 7 patients had reduced left ventricular function (EF < 55%).

3.5. *Effective radiation dose*

The mean total effective radiation exposure that patients received from the dual-source CT scan in single-energy mode was 14.4 ± 2 mSv (Table 5).

So to conclude, our initial study showed significant correlation and good agreement between the findings of DSCT myocardial perfusion defects and the findings of stenosis and its degree on cCTA on a segmental basis with 83% sensitivity, 87% specificity, 86% accuracy, 74% positive predictive value and 92% negative predictive value as well as Cohen's Kappa = 0.67 and prevalence and bias adjusted Kappa = 0.71 emphasizing the high diagnostic value of DSCT myocardial perfusion as compared to cCTA as the gold reference standard, despite that the scan was acquired only at rest.

4. Discussion

Myocardial perfusion imaging has become important in risk stratification of patients with CAD (9). The commonly performed myocardial perfusion imaging techniques as SPECT, cardiac MRI or positron emission tomography (PET) are commonly done first (10) to indicate whether the patients are in need for further coronary artery assessment (11).

In the past decade, Coronary CTA has emerged as a very important advance in noninvasive evaluation of CAD. It can exclude coronary arteries affection with very high negative predictive value (12). It, also, can determine the constituents of atheromatous plaque if present and the degree of luminal stenosis in percentage; yet, it cannot determine the physiologic significance of the stenosis (13).

The crucial value in the diagnostic workup of patients with suspected CAD is the combined assessment of coronary artery and myocardial perfusion (10) from a single imaging technique. Accordingly, many trials were completed decades ago to assess myocardial perfusion status using the early generations of cardiac CT scanners (14). With technical advances MDCT was introduced together with newly applied techniques for detection of acute (15) and chronic (16) myocardial ischemia and this helped the concept of myocardial perfusion assessment by CT examination to flourish again (17).

Thus, morphological assessment of coronary artery luminal patency in combination with myocardial perfusion imaging is

Fig. 3 A 45 year old hypertensive and smoker male patient with known CAD is presented with chest pain. (A) Volume rendered image of cardiac left lateral aspect showing LCx dominance that gives the PDA. (B) Volume rendered image of cardiac right lateral aspect showing RCA proximal part narrow segment. (C) Volume rendered blood pool image of cardiac left antero-lateral aspect showing LCx proximal part narrow segment. (D) Magnified volume rendered blood pool image showing the LCx stenotic segment at its proximal part. (E) cMPR image of RCA showing soft tissue plaque at its proximal segment which is also used to locate reference lines before, at and after the plaque for cross-sectional assessment images creation revealing luminal area of 1.8, 0.4 and 1.2 mm^2, respectively, accounting for 72% luminal area narrowing. (F) cMPR image of LAD showing atherosclerosed vessel with proximal segment predominantly soft tissue plaque and middle segment 2 soft tissue plaques. This image is also used to locate reference lines before, at and after the first plaque for cross-sectional assessment images creation revealing luminal area of 7.9, 4.7 and 3.9 mm^2, respectively, accounting for 29% luminal area narrowing at the plaque site. (G) cMPR image of LAD which is also used to locate reference lines before, at and after the second plaque for cross-sectional assessment images creation revealing luminal area of 4.9, 2.4 and 5.2 mm^2, respectively, accounting for 53% luminal area narrowing at the plaque site. (H) cMPR image of LAD which is also used to locate reference lines before, at and after the third plaque for cross-sectional assessment images creation revealing luminal area of 5, 2.2 and 3.5 mm^2, respectively, accounting for 51% luminal area narrowing at the plaque site. (I) cMPR image of LCx showing atherosclerosed vessel with proximal part soft tissue plaque causing marked narrowing of its lumen which is also used to locate reference lines before, at and after the plaque for cross-sectional assessment images creation revealing luminal area of 5.2, 0.8 and 5.6 mm^2, respectively, accounting for 86% luminal area narrowing at the plaque site. (J) Short axis gray scale image at left ventricle midsegment after narrowing WW and WL (WW: 134 and WL: 100) showing posterior aspect of lateral wall hypo-dense area of hypo-perfusion. (K) Short axis image with applied first pass enhancement tool at the same level as J image emphasizing the myocardial hypo-perfused area that is highlighted by light gray shade. (L) Short axis image with applied late enhancement tool at the same level as J and K images demonstrating the myocardial hypo-perfused area as an area of deep blue color as compared to the surrounding normally perfused myocardium taking light blue or green color. In J, K and L images added ROIs at the hypo-perfused area in the posterior aspect of lateral wall, anterior, septal and posterior walls of the left ventricle showing low mean density at the hypo-perfused area, 47 HU as compared to mean density of other ROIs measuring 93, 88 and 96 HU, respectively. (M) Horizontal long axis image of the left ventricle with applied first pass enhancement tool showing the myocardial hypo-perfused area along the basal, mid and apical segments of the posterior aspect of lateral wall that is highlighted by light gray shade. (N) Vertical long axis image of the left ventricle lateral wall with applied first pass enhancement tool showing the myocardial hypo-perfused area along the basal, mid and apical segments of the lateral wall that is highlighted by light gray shade. Added ROI at the hypo-perfused area shows low mean density at the hypo-perfused area, 47 HU. (O) Short axis image at left ventricle midsegment with applied first pass enhancement tool showing posterior wall myocardial hypo-perfused area that is highlighted by light gray shade.

the ideal to correlate the findings of both imaging (17). Introduction of dual-source CT has enabled to perform cCTA study with high quality (18).

Ruzsics et al., 2008 conducted a systematic study on 35 patients who were subjected to cardiac DSCT scan, using scanner with 2 tubes × 32 detector rows with 64 effective detector rows (Definition, Siemens, Forchheim, Germany) which was operated in dual energy mode and they highlighted its potential usefulness in comprehensive evaluation of coronary artery morphology and stenosis detection and evaluation of myocardial segments perfusion and diagnosis of perfusion deficits (myocardial ischemia) based on a single contrast-enhanced cardiac CT scan operated in dual-energy mode (17).

This study, in contrast to previous studies, was based on the use of one of the most recent and advanced dual source systems using 2 tubes × 128 detector rows with 256 effective detector rows (Somatom Definition Flash; Siemens Healthcare, Forchheim, Germany). This study interpreted and analyzed imaging data of a similar patient population (35 patients) who had performed cardiac DSCT scan operated in single energy mode due to unavailability of heart PBV cardiac CT

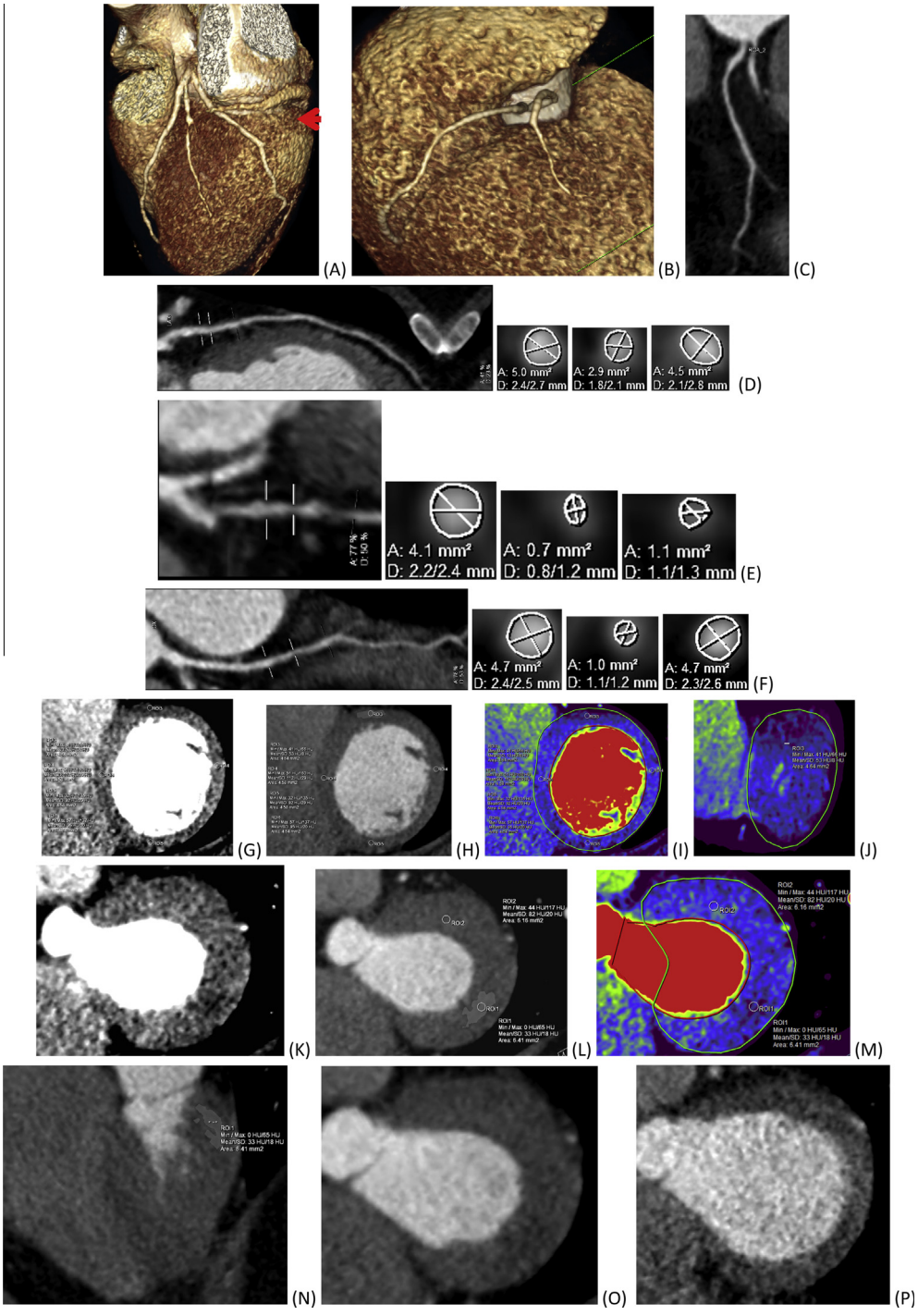

perfusion analysis software and was thus used the only available basic perfusion software.

In their study, Ruzsics et al., 2008 evaluated the coronary artery segments of the studied patients on the cCTA images to identify significant (>50%) coronary artery stenosis. They also evaluated DECT iodine maps to identify myocardial blood pool deficits and they also compared and correlated the findings of segmental myocardial blood pool deficits on DECT iodine maps with the findings of significant stenosis on cCTA and demonstrated that 126/593 myocardial segments have shown perfusion defect and were supplied by a coronary artery with significant (>50%) stenosis. Their study proved that detection of ischemic myocardial segments using DECT iodine maps when compared with cCTA on a segmental basis had 80% sensitivity, 91% specificity and 89% accuracy with 67% PPV and 95% NPP (17).

In the current study, we have also evaluated coronary artery morphology and assessed the degree of the stenosis when found and evaluated myocardial segments perfusion using the gray scale images for subjective diagnosis of perfusion defects which appear hypo-dense in relation to the surrounding normally perfused areas. Furthermore, we observed the color coded contrast attenuation images of the left ventricle that were created by the available first pass and delayed enhancement tools that color overlay the multi-planar reformatted images depending on the amount of iodine based contrast that was perfused into the myocardial tissue with the perfused blood. These colors coded and overlaid images provided a semi-objective way to detect the hypo-perfused areas. In order to evaluate myocardial perfusion objectively, we have placed ROIs in the hypo-perfused myocardial areas as well as the segments that show normal perfusion and compared the numerical data of both.

Correlation of DSCT myocardial perfusion findings and cCTA findings of the studied patient population revealed an overall 83% sensitivity, 87% specificity, 86% accuracy, 70% Youden's index with 74% positive predictive value and 92% negative predictive value. Comparing the statistical analysis data derived from Ruzsics et al., 2008 study (17) results and the statistical analysis data derived from this study results revealed subtle to mild differences as regards sensitivity, specificity, accuracy, PPV and NPV as detailed in Table 6. Our study showed a subtle decrease in specificity, accuracy and NPV (4%, 3% and 3%, respectively) and a slight increase in sensitivity of 3% and PPV of 7%.

The mean total effective radiation exposure that patients received in this study based on dual-source CT scanning while the machine was operated in single-energy mode which is 14.4 ± 2 mSv is slightly lower than that patients received in the study conducted by Ruzsics et al., 2008, which is based on dual-source CT scanning while the machine is operated in dual-energy mode (DECT) which is 15.23 ± 2.7 mSv (17).

From their initial experience, Ruzsics et al., 2008, suggested that patients with known or suspected CAD could be

Fig. 4 A 73 year old male patient with known CAD is presented with chest pain. (A) Volume rendered image of cardiac anterior aspect showing atherosclerotic left main coronary artery, LAD with its first diagonal branch and LCx artery. All shown arteries show surface irregularities with contour bulges. (B) Volume rendered image of cardiac right postero-lateral aspect showing normal variant with the conus branch whish usually arises from the RCA originates directly from the aorta near the origin of the RCA. Both show surface irregularities with contour bulges. (C) cMPR image of RCA showing no lesions. Also, it shows the conus branch (red arrow) comes off directly from the aorta adjacent to RCA origin. (D) cMPR image of LAD showing atherosclerosed vessel with proximal segment soft tissue plaque which is also used to locate reference lines before, at and after the plaque for cross-sectional assessment images creation revealing luminal area of 5, 2.9 and 4.5 mm^2, respectively, accounting for 41% luminal area narrowing at the plaque site. (E) cMPR image of first diagonal branch of LAD showing atherosclerosed vessel with luminal caliber irregularities caused by soft tissue plaques. The image which is also used to locate reference lines before, at and after the most stenotic point for cross-sectional assessment images creation revealing luminal area of 4.1, 0.7 and 1.1 mm^2, respectively, accounting for 77% luminal area narrowing at that point. (F) cMPR image of LCx showing atherosclerosed vessel with soft plaque at its middle segment which is also used to locate reference lines before, at and after the plaque for cross-sectional assessment images creation revealing luminal area of 4.7, 1 and 4.7 mm^2, respectively, accounting for 76% luminal area narrowing at the plaque site. (G) Short axis gray scale image after narrowing WW and WL (WW: 171 and WL: 107) showing anterior wall midsegment hypo-dense area of hypo-perfusion. (H) Short axis image with applied first pass enhancement tool at the same level as G image emphasizing the anterior wall myocardial hypo-perfused area that is highlighted by light gray shade. (I) Short axis image with applied late enhancement tool at the same level as G and H images demonstrating the anterior wall myocardial hypo-perfused area as an area of deep blue color as compared to the surrounding normally perfused myocardium taking light blue or green color. In G, H and I images added ROIs at the anterior wall hypo-perfused area, lateral, posterior and septal walls of the left ventricle showing low mean density at the hypo-perfused area, 53 HU as compared to mean density of other ROIs measuring 112, 92 and 95 HU, respectively. (J) Horizontal long axis image of left ventricle anterior wall with applied late enhancement tool demonstrating the anterior wall myocardial hypo-perfused area as an area of deep blue color. (K) Short axis gray scale image at the base of left ventricle after narrowing WW and WL (WW: 172 and WL: 96) showing postero-lateral hypo-dense area of hypo-perfusion. (L) Short axis image with applied first pass enhancement tool at the same level as K image emphasizing the postero-lateral wall myocardial hypo-perfused area that is highlighted by light gray shade. (M) Short axis image with applied late enhancement tool at the same level as K and L images demonstrating the postero-lateral wall myocardial hypo-perfused area as an area of deep blue color. In L and M images added ROIs at the postero-lateral wall hypo-perfused area and anterior wall of the left ventricle showing low mean density at the hypo-perfused area, 33 HU as compared to mean density of the other ROI measuring 82 HU. (N) Horizontal long axis image of left ventricle with applied first pass enhancement tool demonstrating the basal postero-lateral wall myocardial hypo-perfused area that is highlighted by light gray shade. (O and P) Short axis gray scale images at left ventricular basal level at end-systole and end-diastole, respectively, showing no kinetic abnormalities.

non-invasively evaluated using dual source CT scanners with independent operation of both tubes in dual energy mode (DECT) for concomitant evaluation of their coronary arteries to confirm or rule out significant coronary disease using cCTA and evaluation of myocardial perfusion for perfusion deficits using DECT iodine maps in the same setting and single CT scan acquisition (17).

We, also, propose that comprehensive evaluation of coronary artery morphology and myocardial perfusion could be achieved by single non-invasive contrast enhanced CT acquisition using DSCT scanners while operated in single energy mode with high sensitivity and specificity as well as high diagnostic accuracy.

5. Study limitations

Relatively small number of the studied cohort population need to involve larger number of patients in future studies for better validation of our findings. We also had a concern on the fact that study was acquired only at rest without application of any stress to myocardium.

5.1. Clinical implications

With application of the suggested technique, we could evaluate both myocardial perfusion and coronary artery luminal

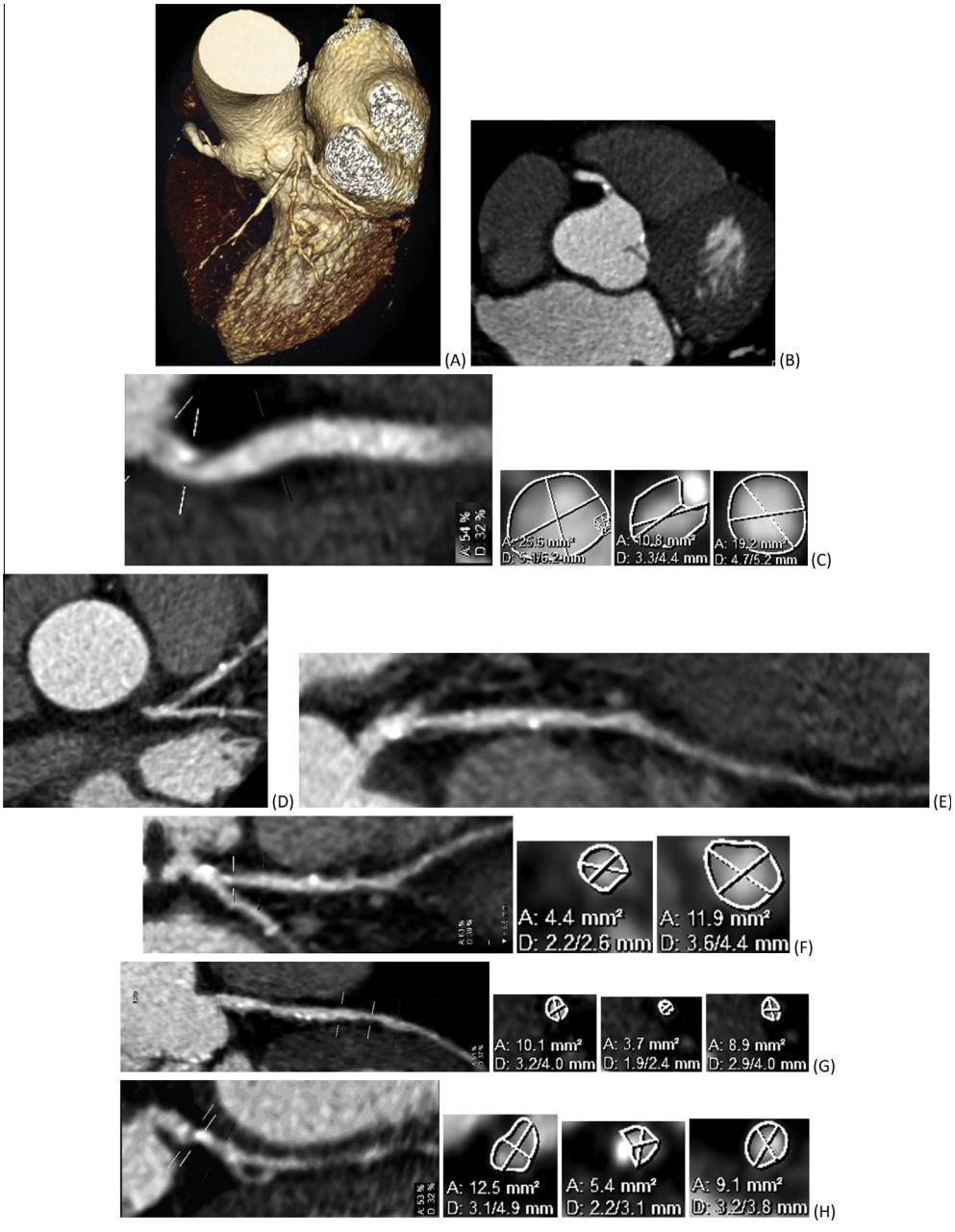

patency at the same time with single contrast enhanced CT acquisition with the same amount of contrast material as coronary CT angiography study alone and with lower radiation exposure.

6. Conclusion

The suggested technique is a comprehensive correlative reproducible non-invasive contrast enhanced CT study with low radiation dose. It combines myocardial perfusion evaluation and coronary morphological evaluation without increasing the used contrast material and with good correlation increasing the diagnostic information and accuracy of the study more than that of the coronary CT angiography alone.

We suggest that DSCT myocardial perfusion imaging has the potential to be the first, independent and stand out imaging choice for comprehensive and correlative assessment of both myocardial perfusion status and coronary arterial morphology in patients with suspected or known CAD.

Future validation of the suggested technique in correlation with computationally derived fractional flow reserve (FFR_{CTA}) studies could surely add more valuable information regarding the hemodynamic of coronary blood flow and myocardial perfusion dynamics.

Conflict of interest

The authors declare that there are no conflict of interests.

Fig. 5 A 76 year old male patient with known CAD is presented with chest pain. (A) Volume rendered blood pool image of cardiac anterior aspect showing atherosclerotic left main coronary artery that trifurcates into LAD, ramus intermedius and LCx arteries. All shown arteries show surface irregularities with contour bulges. (B) Row data source image showing RCA proximal segment mixed (soft and calcific) plaque seen near its origin. (C) cMPR image of RCA showing atherosclerotic ecstatic RCA with mixed osteal plaque which is also used to locate reference lines before, at and after the plaque for cross-sectional assessment images creation revealing luminal area of 25.6, 10.8 and 19.2 mm^2, respectively, accounting for 54% luminal area narrowing at the plaque site. (D) Row data source image showing LAD osteal plaque (red arrow). (E) cMPR image of LAD showing atherosclerosed vessel with osteal and midsegment soft tissue plaques (red arrows). (F) cMPR image of LAD showing atherosclerosed vessel with osteal soft tissue plaque which is also used to locate reference lines before, at and after the plaque for cross-sectional assessment images creation revealing luminal area of 4.4 and 11.9 mm^2, respectively, accounting for 63% luminal area narrowing at the plaque site. (G) cMPR image of LAD showing atherosclerosed vessel with soft tissue plaque at its midsegment which is also used to locate reference lines before, at and after the plaque for cross-sectional assessment images creation revealing luminal area of 10.1, 3.7 and 8.9 mm^2, respectively, accounting for 51% luminal area narrowing at the plaque site. (H) cMPR image of LCx showing atherosclerosed vessel with calcific plaque at its proximal segment which is also used to locate reference lines before, at and after the plaque for cross-sectional assessment images creation revealing luminal area of 12.5, 5.4 and 9.1 mm^2, respectively, accounting for 53% luminal area narrowing at the plaque site. (I) Short axis gray scale image after narrowing WW and WL (WW: 199 and WL: 109) showing posterior wall midsegment hypo-dense area of hypo-perfusion. (J) Short axis image with applied first pass enhancement tool at the same level as I image emphasizing the posterior wall myocardial hypo-perfused area that is highlighted by light gray shade. (K) Short axis image with applied late enhancement tool at the same level as I and J images demonstrating the posterior wall myocardial hypo-perfused area as an area of deep blue color as compared to the surrounding normally perfused myocardium taking light blue or green color. In I, J and K images added ROIs at the posterior wall hypo-perfused area, lateral, anterior and septal walls of the left ventricle showing low mean density at the hypo-perfused area, 43 HU as compared to mean density of other ROIs measuring 87, 80 and 92 HU, respectively. (L) Short axis gray scale image after narrowing WW and WL (WW: 199 and WL: 109) showing anterior wall midsegment hypo-dense area of hypo-perfusion. (M) Short axis image with applied first pass enhancement tool at the level as L image emphasizing the anterior wall myocardial hypo-perfused area that is highlighted by light gray shade. (N) Vertical long axis image after narrowing WW and WL (WW: 199 and WL: 109) and applied first pass enhancement tool showing the anterior wall myocardial hypo-perfused area that is highlighted by light gray shade. (O) Short axis image with applied late enhancement tool at the same level as L and M images demonstrating the anterior wall myocardial hypo-perfused area as an area of deep blue color. In L, M and O short axis images, ROIs are added at the anterior wall hypo-perfused area, lateral, septal and posterior walls of the left ventricle showing low mean density at the hypo-perfused area, 43 HU as compared to mean density of other ROIs measuring 109, 103 and 84 HU, respectively. Second posterior wall small ROI is added over a small posterior wall hypo-perfused focus seen lateral to the posterior wall reference ROI and shows low mean density at the hypo-perfused focus; 54 HU. (P) Short axis gray scale image after narrowing WW and WL (WW: 190 and WL: 100) showing lateral wall basal segment hypo-dense area of hypo-perfusion. (Q) Short axis image with applied first pass enhancement tool at the same level as P image emphasizing the lateral wall myocardial hypo-perfused area that is highlighted by light gray shade. (R) Short axis image with applied late enhancement tool at the same level as P and Q images demonstrating the lateral wall myocardial hypo-perfused area as an area of deep blue color. In P, Q and R images added ROIs at the lateral wall hypo-perfused area, anterior and posterior walls of the left ventricle showing low mean density at the hypo-perfused area, 37 HU as compared to mean density of other ROIs measuring 95 and 86 HU, respectively. (S and T) Short axis images at left ventricular midsegment level at end-systole and end-diastole, respectively, showing hypo-kinesia of septal, posterior and lateral walls of left ventricle. (U) 17 segment map of left ventricular myocardial motion shows kinetic abnormalities with segments of akinesia or sever hypo-kinesia demonstrated in purple color and segments of hypo-kinesia demonstrated in blue color as compared to good motion demonstrated in green and red colors. (V) 17 segment map of left ventricular myocardial thickening shows segments of weak and poor myocardial thickening which are demonstrated in blue and purple colors. Ejection fraction of this case was a little bit sub-optimal 52% (Normal range is 56–78%).

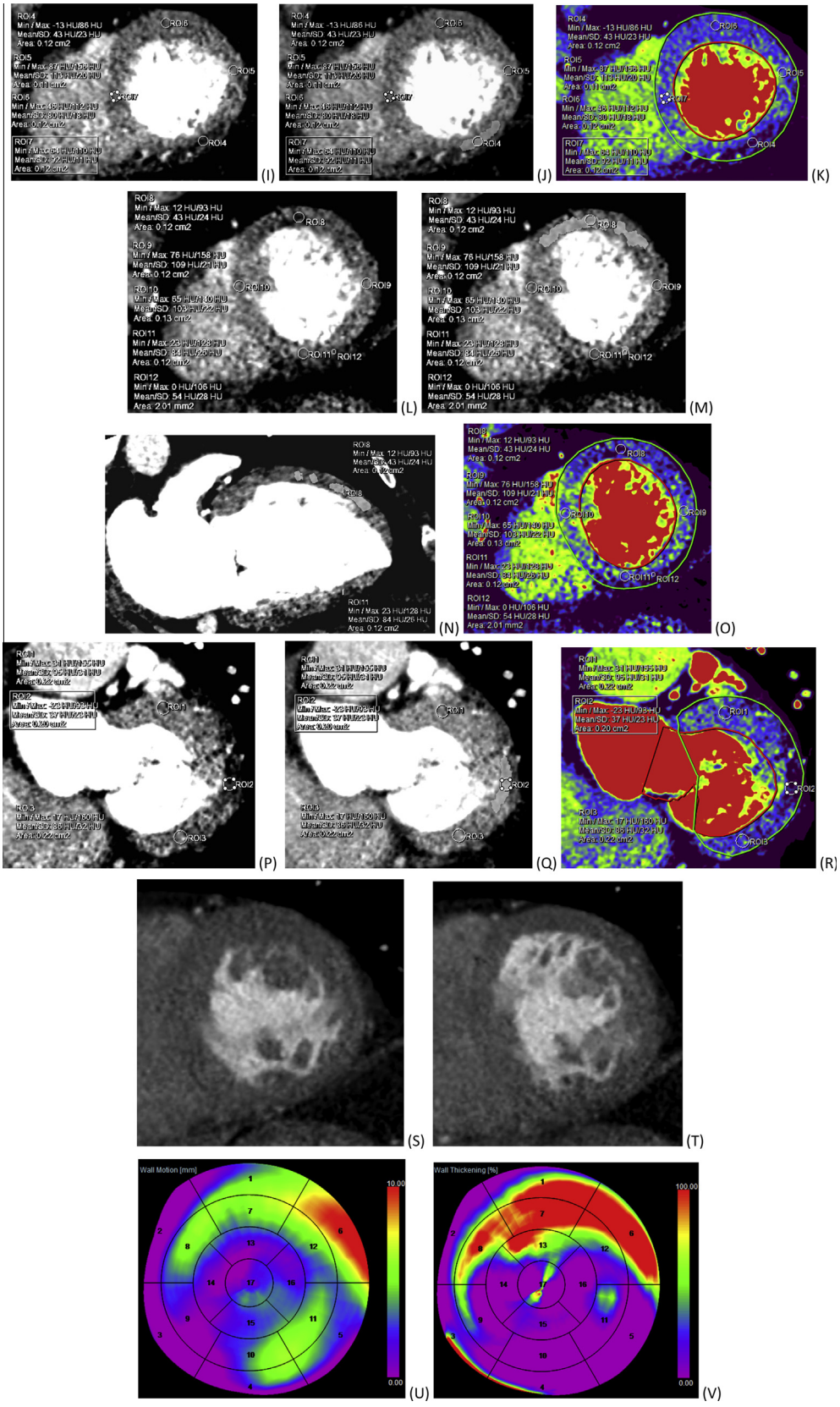

Fig 5 *(continued)*

Table 4 Per segment analysis for the diagnostic value of DSCT.

		Perfusion defect by DSCT		
		Positive	Negative	Total
Significant lesion by cCTA	Positive	154	31	185
	Negative	55	355	410
	Total	209	386	595
Index	Estimate	SE	Lower 95% CI	Upper 95% CI
Sensitivity	0.83	0.03	0.77	0.88
Specificity	0.87	0.02	0.83	0.90
Accuracy	0.86	0.01	0.82	0.88
Youden's index	0.70	0.03	0.64	0.76
Positive predictive value	0.74	0.03	0.67	0.80
Negative predictive value	0.92	0.01	0.89	0.94
Cohen's Kappa	0.67	0.03	0.61	0.74
Prevalence and bias adjusted Kappa	0.71			

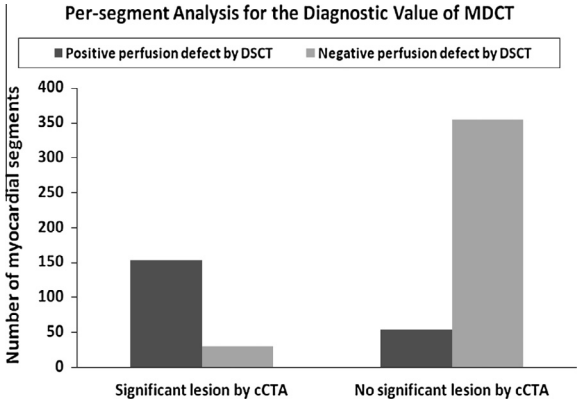

Fig. 6 Per-segment analysis for the diagnostic value of DSCT.

Table 5 Values of effective radiation dose received by the patients.

Variable	n.	Min.	Max.	Mean	SD	Percentiles		
						25th	50th	75th
Effective radiation dose (mSv)	35	11.0	18.2	14.4	2.0	12.8	14.2	16.0

Table 6 Comparison between statistical analysis results of Ruzsics et al., 2008, study and our study. PPV and NPV stand for positive and negative predictive value.

Index	Ruzsics et al., 2008 (%)	Our study (%)	Difference (%)
Sensitivity	80	83	↑ 3
Specificity	91	87	↓ 4
Accuracy	89	86	↓ 3
PPV	67	74	↑ 7
NPP	95	92	↓ 3

Acknowledgments

We would like to thank CT technologists Mohammad Salah-Edden Zain-Alabedeen and Mostafa Ismael Nasef for their assistance in this work.

References

(1) Jacobs AK, Antman EM, Ellrodt G, et al. Recommendation to develop strategies to increase the number of ST-segment-elevation myocardial infarction patients with timely access to primary percutaneous coronary intervention. Circulation 2006;113:2052–63.
(2) Antman EM, Anbe DT, Armstrong PW, et al. ACC/AHA guide lines for the management of patients with ST-elevation myocardial infarction: executive summary—a report of the ACC/AHA task force on practice guidelines. Circulation 2004;110:588–636.
(3) Sparrow PJ, Merchant N, Provost YL, et al. CT and MR imaging findings in patients with acquired heart disease at risk for sudden cardiac death. RadioGraphics 2009;29:805–23.
(4) Ghostine S, Caussin C, Habis M, et al. Non-invasive diagnosis of ischemic heart failure using 64-slice computed tomography. Eur Heart J 2008;29:2033–40.
(5) Masci PG, Dymarkowski S, Rademakers FE, et al. Determination of regional ejection fraction in patients with myocardial infarction by using merged late gadolinium enhancement and cine MR: feasibility study. Radiology 2009;250:50–60.
(6) Ricardo CC, Koen N, Michael DS. Comprehensive assessment of myocardial perfusion defects, regional wall motion, and left ventricular function by using 64-section multidetector CT. Radiology 2008;248:466–75.
(7) Ropers D, Rixe J, Anders K, et al. Usefulness of multidetector row spiral computed tomography with 64- x 0.6-mm collimation and 330-ms rotation for the noninvasive detection of significant coronary artery stenoses. Am J Cardiol 2006;97:343–8.
(8) Mackinnon A. A spreadsheet for the calculation of comprehensive statistics for the assessment of diagnostic tests and inter-rater agreement. Comput Biol Med 2000;30(3):127–34.
(9) Berman DS, Hachamovitch R, Shaw LJ, et al. Roles of nuclear cardiology, cardiac computed tomography, and cardiac magnetic resonance: assessment of patients with suspected coronary artery disease. J Nucl Med 2006;47:74–82.

(10) Hachamovitch R, Di Carli MF. Nuclear cardiology will remain the ''gatekeeper''over CT angiography. J Nucl Cardiol 2007;14:634–44.
(11) Klocke FJ, Baird MG, Lorell BH, et al. ACC/AHA/ASNC guidelines for the clinical use of cardiac radionuclide imaging–executive summary: a report of the American College of Cardiology/American Heart Association Task Force on Practice Guidelines (ACC/AHA/ASNC Committee to Revise the 1995 Guidelines for the Clinical Use of Cardiac Radionuclide Imaging). Circulation 2003;108:1404–18.
(12) Meijboom WB, Meijs MF, Schuijf JD, et al. Diagnostic accuracy of 64-slice computed tomography coronary angiography: a prospective, multicenter, multivendor study. J Am Coll Cardiol 2008;52:2035–44.
(13) George RT, Arbab-Zadeh1 A, Cerci RJ, et al. Diagnostic performance of combined noninvasive coronary angiography and myocardial perfusion imaging using 320-MDCT: the CT angiography and perfusion methods of the CORE320 multicenter multinational diagnostic study. AJR 2011;197:829–37.
(14) Rumberger JA, Feiring AJ, Lipton MJ, et al. Use of ultrafast computed tomography to quantitate regional myocardial perfusion: a preliminary report. J Am Coll Cardiol 1987;9:59–69.
(15) George RT, Jerosch-Herold M, Silva C, et al. Quantification of myocardial perfusion using dynamic 64-detector computed tomography. Invest Radiol 2007;42:815–22.
(16) Lardo AC, Cordeiro MA, Silva C, et al. Contrast enhanced multidetector computed tomography viability imaging after myocardial infarction: characterization of myocyte death, microvascular obstruction, and chronic scar. Circulation 2006;113:394–404.
(17) Ruzsics B, Lee H, Powers ER, et al. Myocardial ischemia diagnosed by dual-energy computed tomography: correlation with single-photon emission computed tomography. Circulation 2008;117:1244–5.
(18) Matt D, Scheffel H, Leschka S, et al. Dual-source CT coronary angiography: image quality, mean heart rate, and heart rate variability. AJR 2007;189:567–73.